Vibrational Optical Activity of (S)-1-d-Ethanol

R. A. Shaw, H. Wieser, Remo Dutler, and Arvi Rauk*

Contribution from the Department of Chemistry, University of Calgary, Calgary, Alberta T2N 1N4, Canada. *Received December 19, 1989*

Abstract: Ethanol and (*S*)-*1*-*d*-ethanol have been investigated by ab initio molecular orbital calculations and by experimental measurements of IR and VCD spectra. The structures and relative energies of the *anti* and *gauche* conformers have been determined, including corrections for zero-point vibrational energy. Ethanol exists as 42:58 mixture of *anti*:*gauche* forms. The *gauche* rotamers are inherently chiral structures, and their VCD spectra have been determined by ab initio application of vibronic coupling theory. Deuterium substitution of the *pro-S* hydrogen atom results in a slight preference for the *M* rotamer over the *P* form because of the lower zero-point vibrational energy of the former. The IR spectrum of ethanol and the IR and VCD spectra of (*S*)-*1*-*d*-ethanol have been determined theoretically by application of the vibronic coupling formalism of Nafie and Freedman, and the experimental VCD spectrum of (*S*)-*1*-*d*-ethanol has been measured in the 800–1350-cm^{-1} range. Some features of the spectrum may be attributed to the absolute configuration at the asymmetric carbon atom, independent of conformation, while others are associated with the chirality of the *gauche* forms of the compound.

Introduction

α-Deuterioethanol is one of the earliest compounds synthesized which is rendered optically active by virtue of isotopic substitution.[1,2] The absolute configuration was determined by Lemieux and Howard[3] as (*R*)-(+)-α-*d*-ethanol. The compound has proved useful as a mechanistic and stereochemical probe in biochemical reactions.[4] Ethanol exists as an equilibrium mixture of an optically inactive *anti* rotamer and a racemic mixture of the enantiomeric *gauche* rotamers. The free energy difference between the two structures has been estimated from microwave measurements to be 0.49 ± 0.06 kJ/mol,[5] favoring the *anti* rotamer. Resolved α-*d*-ethanol exists as mixture of three distinct diastereomeric conformations, the *anti* form, and (*P*)- and (*M*)-*gauche* forms. The two *gauche* forms are energetically inequivalent by virtue of different zero-point vibrational energies. The composition of the equilibrium mixture of the α-*d*-ethanol has not been determined experimentally. A number of ab initio investigations of the structure of ethanol have been carried out,[6-8] but these have not been of sufficient accuracy to determine the relative energies of the two forms reliably. The IR spectra of ethanol and all of the deuterated isotopomers have been investigated experimentally by Perchard and Josien.[9] Intensities of the harmonic normal modes have been estimated from transferred atomic polar tensors and force constants by Person[10] who did not discuss the question of the composition of the equilibrium mixture. Vibrational circular dichroism (VCD) measurements in the C-H and C-D stretching region have been carried out on α-*d*- and α,*O*-d_2-ethanol, and in the mid-IR for the latter compound by Pultz.[11] In view of the intrinsic importance of ethanol and its α-*d* isotopomer, we undertook to carry out a complete analysis of the IR and VCD spectra of the two systems.

We report here an ab initio determination of the structure and relative energies of the *anti* and *gauche* conformers of ethanol and optically active (*S*)-*1*-*d*-ethanol. A scaled quantum mechanical force field for the deuterated and undeuterated conformers is determined from careful scaling to match the IR data of Perchard and Josien.[9] The vibronic coupling theory of Nafie and Freedman[12] is applied to determine the IR intensities of the parent compound and the IR and VCD intensities of the optically active isotopomer. We also report the first measurement of the VCD spectrum of (*S*)-*1*-*d*-ethanol in the mid-IR. While this work was in progress,[13] the results of a similar investigation by Dothe, Lowe, and Alper (DLA) appeared.[14] DLA applied the ab initio formalism of Stephens[15] for the calculation of IR and VCD intensities of the same system. The present work differs from that of DLA in several important respects, beside the theoretical method for IR and VCD intensities, and the measurement of the VCD spectrum. These differences will be discussed in due course.

Theoretical Details

The following is an abbreviated derivation of the vibronic coupling theory of Nafie and Freedman[12] which has been implemented at the ab initio level by Dutler and Rauk.[16,17] The dipole strength, $D_{g,e}$, and rotational strength, $R_{g,e}$, are given by:

$$D_{g,e} = (\mu)_{g,e}(\mu)_{e,g} = ((\Phi_g|\mu_{el}|\Phi_e\rangle(\Phi_e|\mu_{el}|\Phi_g\rangle) \quad (1)$$

$$R_{g,e} = (\mu)_{g,e}(m)_{e,g} = \mathrm{Im}((\Phi_g|\mu_{el}|\Phi_e\rangle(\Phi_e|\mu_{mag}|\Phi_g\rangle) \quad (2)$$

where Φ_g and Φ_e are the total molecular wave function of the ground-state g and a vibrationally excited state e. The operators μ_{el} and μ_{mag}, the electric and magnetic dipole operators, are given by:

$$\mu_{el} = \mu^n_{el} + \mu^e_{el} = \sum_{n=1}^{n=n_{atoms}} \xi_n r_n + \sum_{i=1}^{i=n_{electrons}} \xi_i r_i \quad (3)$$

$$\mu_{mag} = \mu^n_{mag} + \mu^e_{mag} = \sum_{n=1}^{n=n_{atoms}} \frac{\xi_n}{2m_n c}(r_n \times p_n) + \sum_{i=1}^{i=n_{electrons}} \frac{\xi_i}{2m_i c}(r_i \times p_i) \quad (4)$$

where μ^n_{el}, μ^e_{el}, μ^n_{mag}, and μ^e_{mag} denote the nuclear and electronic contributions of the electric and magnetic dipole transition moment operators, respectively. ξ_k is the charge of particle k with mass

(1) Levy, H. R.; Loewus, F. A.; Vennesland, J. M. *J. Am. Chem. Soc.* **1957**, *79*, 2949.
(2) For a review, see: Verbit, L. *Prog. Phys. Org. Chem.* **1970**, *7*, 51-127.
(3) Lemieux, R. U.; Howard, J. *Can. J. Chem.* **1963**, *41*, 308.
(4) Eksirom, G.; Norsten, C.; Cronholm, T.; Ingelman-Sundberg, M. *Biochemistry* **1987**, *26*, 7348-7354 and references therein.
(5) Kakar, R. K.; Quade, C. R. *J. Chem. Phys.* **1980**, *72*, 4300-4307.
(6) (a) French, M. A.; Ikuta, S.; Kebarle, P. *Can. J. Chem.* **1982**, *60*, 1907-1918. (b) Hopkinson, A. C.; Lien, M. H. *THEOCHEM* **1983**, *9*, 153-166. (c) Tolosa Arroyo, S.; Olivares del Valle, F. J. *An. Fis., Ser. A* **1983**, *79*, 112-120. (d) Ohsaku, M.; Ichiishi, T.; Imamura, A.; Hayashi, M. *Bull. Chem. Soc. Jpn.* **1984**, *57*, 2791-6. (e) Teixeira-Dias, J. J. J.; Fausto, R. *J. Mol. Struct.* **1986**, *144*, 199-213.
(7) Murto, J.; Rasanen, M.; Aspiala, A.; Lotta, T. *THEOCHEM* **1984**, *17*, 99-112.
(8) (a) Schaefer, L.; Van Alsenoy, C.; Scarsdale, J. N. *J. Mol. Struct.* **1982**, *86*, 349. (b) Van Alsenoy, C.; Scarsdale, J. N.; Williams, J. O.; Schaefer, L. *THEOCHEM* **1982**, *3*, 365-376. (c) Siam, K.; Ewbank, J. D.; Schaefer, L.; Van Alsenoy, C.; Allinger, N. L. *THEOCHEM* **1986**, *32*, 83-99.
(9) Perchard, J.-P.; Josien, M.-L. *J. Chim. Phys. Phys.-Chim. Biol.* **1968**, *65*, 1834-1875.
(10) Person, W. B. *Report* **1982**, N-82-25047 (*Chem. Abstr.* **1982**, 99:130590x).
(11) Pultz, V. M. Vibrational Circular Dichroism Studies of Some Small Chiral Molecules. Ph.D. Dissertation, University of Minnesota, 1983.
(12) Nafie, L. A.; Freedman, T. B. *J. Chem. Phys.* **1983**, *78*, 7108.
(13) Part of the present work has been reported elsewhere: Dutler, R.; Rauk, A.; Shaw, R. A.; Wieser, H. Presented at 10th Canadian Symposium on Theoretical Chemistry, Banff, Canada, Aug 24-30, 1989.
(14) Dothe, H.; Lowe, M. A.; Alper, J. S. *J. Phys. Chem.* **1989**, *93*, 6632-6637.
(15) Stephens, P. J. *J. Phys. Chem.* **1985**, *89*, 748-752.
(16) Dutler, R. Ph.D. Dissertation, The University of Calgary, 1988.
(17) Dutler, R.; Rauk, A. *J. Am. Chem. Soc.* **1989**, *111*, 6957-6966.

0002-7863/90/1512-5401$02.50/0

m_k which is located at a point r_k relative to the origin of coordinates and moving with linear momentum p_k. The wave functions Φ_e and Φ_g may be represented as $\Phi_{0\nu'}$ and are expanded in terms of adiabatic Born–Oppenheimer functions $\{\Psi^a_e(r, Q)\phi_{e\nu}(Q)\}$:

$$\Phi_{0\nu'} = \Psi^a_0\phi_{0\nu'} - \sum_{e\nu} \frac{(\Psi^a_e\phi_{e\nu}|\hat{T}_N|\Psi^a_0\phi_{0\nu'})}{E_{e\nu} - E_{0\nu'}} \quad (5)$$

The variable ν' is either 0 or 1, denoting the vibrational ground or first excited state. The perturbation operator $\hat{T}_N$ is taken as that part of the nuclear kinetic energy operator which involves only first derivatives with respect to nuclear coordinates (normal modes) Q, acting separately on the electronic and nuclear parts of wave function, namely

$$\hat{T}_N = -\left(\frac{h}{2\pi}\right)^2\left(\frac{\partial}{\partial Q}\right)_{elec}\left(\frac{\partial}{\partial Q}\right)_{nuc} \quad (6)$$

The normal mode dependence of Ψ^a_0 is expressed as a Taylor expansion about the equilibrium geometry, keeping only the first-order terms, and using the identity $1 = \sum_e|\Psi^a_e\rangle\langle\Psi^a_e|$,

$$\Psi^a_0 = (\Psi^a_0)_0 + \left(\frac{\partial\Psi^a_0}{\partial Q}\right)_0 Q = (\Psi^a_0)_0 + \sum_e \langle\Psi^a_e|\frac{\partial}{\partial Q}|\Psi^a_0\rangle_0 Q\Psi^a_e \quad (7)$$

Use of eqs 3–7, the approximation that the separation between vibrational levels of different electronic states is approximately-equal to the difference between Born–Oppenheimer surfaces at the ground-state equilibrium geometry, namely

$$\frac{1}{E_{e\nu} - E_{01}} = \frac{1}{E^0_e - E^0_0} \quad (8)$$

and the expansion of the normal modes in terms of internal coordinates R_n,

$$Q^j = \sum_{n=1}^{n_{atoms}} R_n s^j{}_n \quad (9)$$

allows one to obtain, after some algebra, expressions for the electric and magnetic dipole transition moments used in eq 1 and 2. Specifically, for the jth normal mode, one obtains[12]

$$\mu^{VC}_{(00,01)j} = \left(\frac{\hbar}{2\omega_j}\right)^{1/2}\left[\sum_{n=1}^{n_{atoms}} \xi_n s^j{}_n - 2\sum_{n=1}^{n_{atoms}}\sum_{i=1}^{n_{electrons}}\sum_{e=1}^{n_{ex}} \langle\Psi^a_0|r_i|\Psi^a_e\rangle\langle\Psi^a_e|\frac{\partial}{\partial R_n}|\Psi^a_0\rangle S^j{}_n\right] \quad (10.1)$$

$$| = \left(\frac{\hbar}{2\omega_j}\right)^{1/2}\left[\sum_{n=1}^{n_{atoms}} \xi_n s^j{}_n - 2\sum_{n=1}^{n_{atoms}}\sum_{i=1}^{n_{electrons}} \langle\Psi^a_0|r_i\frac{\partial}{\partial R_n}|\Psi^a_0\rangle s^j{}_n\right] \quad (10.2)$$

and

$$m^{VC}_{(00,01)j} = \frac{1}{2c}\left(\frac{\hbar}{2\omega_j}\right)^{1/2}\left[i\sum_{n=1}^{n_{atoms}} \xi_n(R_n \times s^j{}_n) - 2\sum_{n=1}^{n_{atoms}}\sum_{i=1}^{n_{electrons}}\sum_{e=1}^{n_{ex}} \langle\Psi^a_0|r_i \times p_i|\Psi^a_e\rangle\langle\Psi^a_e|\frac{\Delta}{\Delta R_n}|\Psi^a_0\rangle s^j{}_n\frac{1}{E^0_e - E^0_0}\right] \quad (11)$$

The superscript VC denotes that these expressions describe a vibronic coupling mechanism for IR and VCD intensities. The subscript (00,01) signifies that the transition is between the $\nu = 0$ and $\nu = 1$ vibrational levels of the ground electronic state of the molecule. Electric dipole strengths derived from eq 10 are formally equivalent to the atomic polar tensor (APT) theory. Stephens circumvents the summation over excited states in eq 11 by invoking the magnetic field dependence of the wave function, a procedure which requires solution of the perturbed Hartree–Fock equations in the presence of a magnetic field.[15] In the present case, the sum over excited states which appears in eq 10.2 and in the second term of eq 11 is explicitly evaluated, in the first instance as a check for the "completeness" of the set of excited states (i.e., eq 10.1 and 10.2 should yield identical results), and in the second case out of necessity, since the presence of the energy dependence within the summation in eq 11 precludes closure as is possible for eq 10. "Completeness" by the criterion that eq 10.1 and 10.2 give nearly identical results is only satisfied if the basis set is expanded by addition to it of derivatives of the normal basis functions with respect to nuclear displacements.[18]

Computational Details

The geometries and relative energies of the *anti* and *gauche* rotamers of ethanol were determined by complete optimization at the restricted Hartree–Fock level of theory using the analytical procedures of the GAUSSIAN 86 system of programs[19] and the internal 6-31G*, 6-31G**, and 6-31+G** basis sets. At each level, the correlation correction was determined up to fourth order in Moller–Plesset perturbation theory (MP4). Normal coordinate analysis at each of the equilibrium geometries was carried out by analytical second differentiation of the Born–Oppenheimer RHF energy using the corresponding basis set. In addition, the geometries of the *gauche* and *anti* forms were optimized and normal coordinate analyses carried out using a basis set we designate as 6-31G~ (see below) using a modified version of GAUSSIAN 82.[20] Harmonic frequencies for isotopically substituted species, as well as IR and VCD (where appropriate) intensities, were accomplished by the program system Freq85,[16] which implements the vibronic coupling theory of Nafie and Freedman[12] at the ab initio level. The ab initio force fields were scaled to improve agreement of the calculated frequencies with experiment as described below. The intensity evaluations were accomplished using the 6-31G~ basis set, which is constructed by addition to the 6-31G basis set all nonredundant derivatives of the 6-31G basis functions with respect to nuclear displacements.[18] Previous experience[16,17,21] has shown that 6-31G~ geometries are very similar to 6-31G** geometries, and the present experience confirms this observation. The origin of coordinates in all intensity calculations was the molecular center of mass. Except as noted, simulated IR and VCD spectra were obtained assuming a Lorentzian line shape of half-width 5 and 8 cm^{-1}, respectively. Frequencies used in the simulated spectra were calculated from the empirically scaled quantum mechanical force field.

Experimental Details

A sample of (*S*)-α-*d*-ethanol was provided by T. Cronholm with the following composition:[4] undeuterated, 9.3%; (*R*)-*1*-*d*, 4.1%; (*S*)-*1*-*d*, 81.8%; 1,1-d_2, 4.7%. The molar absorptivity scale in the plotted VCD spectra has been corrected for the composition. Samples of (*R*)-α-*d*-ethanol provided by T. Cronholm and H. S. Mosher proved to have too much *O*-deuteration for reliable VCD measurement.

All spectra were measured using a Nicolet 8000 FT-IR spectrometer modified for VCD measurements as outlined by Nafie and Diem.[22] The VCD components included a KRS-5 linear polarizer (Cambridge Instruments), ZnSe photoelastic modulator (Hinds International) operating at 37 kHz, a lock-in amplifier (Stanford Research Model SR 530) with an input time constant of 1 ms, and an optical filter (OCL1) to isolate the 800–1500-cm^{-1} spectral range. Focussing mirrors following the sample were replaced by an $f/1$ ZnSe lens to minimize absorption-dependent artifacts, as recommended by Malon and Keiderling.[23] Spectra were obtained by subtracting the "VCD spectrum" of the solvent alone from that of the sample solution. This method efficiently removes artifacts that arise through polarization-dependent reflection or transmission selectivity, i.e., instrumental artifacts. In our experience, it is crucial to ensure that the polarization bias of the instrument is such that both the base line and single-enantiomer VCD spectra are well displaced from the $\Delta A = 0$ line, since artifacts that originate with the standard phase correction routines will arise if the spectrum approaches zero intensity or changes in sign. Following these precautions, we have successfully reproduced the published VCD spectrum of α-pinene[24] using a single enantiomer. We have further used the technique to measure the spectra

(18) (a) Sadlej, A. J. *Chem. Phys. Lett.* **1977**, *47*, 50. (b) Nakatsuji, H.; Kanda, K.; Yonezawa, T. *Chem. Phys. Lett.* **1980**, *75*, 340.
(19) Frisch, M. J.; Binkley, J. S.; Schlegel, H. B.; Raghavachari, K.; Melius, C. F.; Martin, L. R.; Stewart, J. J. P.; Bobrowicz, F. W.; Rohlfing, C. M.; Kahn, L. R.; De Frees, D. J.; Seeger, R.; Whiteside, R. A.; Fox, D. J.; Fleuder, E. M.; Pople, J. A. Carnegie-Mellon Publishing Unit: Pittsburgh, PA, 1984.
(20) (a) Binkley, J. S.; Frisch, M. J.; Defrees, D. J.; Raghavachari, K.; Whitesides, R. A.; Schlegel, H. B.; Fluder, E. M.; Pople, J. A., Department of Chemistry, Carnegie-Mellon University, Pittsburgh, PA. (b) Rauk, A.; Duller, R. *J. Comput. Chem.* **1987**, *8*, 324.
(21) Rauk, A.; Duller, R.; Yang, D. *Can. J. Chem.* **1990**, *68*, 258–266.
(22) Nafie, L. A.; Diem, M. *Appl. Spectrosc.* **1979**, *33*, 130–135.
(23) Malon, P.; Keiderling, T. A. *Appl. Spectrosc.* **1988**, *42*, 32–38.
(24) Lippard, E. D.; Nafie, L. A. *Appl. Spectrosc.* **1984**, *38*, 774.

Table I. Calculated Geometries of the *anti* and *gauche* Conformers of Ethanol[a]

	anti-ethanol					*gauche*-ethanol			
parameter[b]	6-31G*	6-31G**	6-31+G**	6-31G~	exp[c]	6-31G*	6-31G**	6-31+G**	6-31G~
a	1.405	1.404	1.406	1.416	1.431	1.404	1.403	1.405	1.415
b	1.516	1.515	1.515	1.514	1.512	1.521	1.521	1.521	1.518
c	0.947	0.943	0.943	0.942	0.971	0.947	0.943	0.943	0.942
d	1.089	1.090	1.089	1.086	1.098	1.082	1.083	1.083	1.080
e	1.089	1.090	1.089	1.086	1.098	1.089	1.089	1.089	1.086
f	1.086	1.086	1.086	1.084	1.088	1.086	1.086	1.087	1.084
g	1.084	1.084	1.085	1.082	1.091	1.085	1.085	1.085	1.082
h	1.084	1.084	1.085	1.082	1.091	1.087	1.088	1.088	1.085
ab	108.0	108.1	108.3	108.1	107.8	112.5	112.5	112.6	112.5
ac	109.7	109.9	110.7	110.6	105.4	109.4	109.6	109.5	110.4
ad	110.6	110.7	110.3	110.3	110.7	105.8	105.9	105.6	105.6
ae	110.6	110.7	110.3	110.3	110.7	110.6	110.7	110.3	110.2
bd	110.1	110.0	110.1	110.3		110.2	110.1	110.3	110.4
be	110.1	110.0	110.1	110.3		110.3	110.2	110.3	110.5
bf	110.7	110.6	110.4	110.6	110.5	110.9	110.8	110.6	110.6
bg	110.3	110.3	110.4	110.5	110.1	110.3	110.4	110.5	110.6
bh	110.3	110.3	110.4	110.5	110.1	111.1	111.1	111.1	111.1
de	107.5	107.4	107.8	107.7	108.0	107.3	107.2	107.4	107.4
fg	108.6	108.6	108.6	108.5	108.8	108.6	108.6	108.6	108.6
fh	108.6	108.6	108.6	108.5	108.8	107.7	107.7	107.8	107.8
gh	108.3	108.3	108.3	108.2	108.4	108.1	108.1	108.2	108.1
abd	120.2	120.2	120.1	120.1		117.7	117.9	117.7	117.7
abe	−120.2	−120.2	−120.1	−120.1		−124.0	−124.1	−123.7	−123.7
abf	180.0	180.0	180.0	180.0		−177.7	−177.7	−177.7	−177.6
abg	−59.8	−59.8	−58.9	−59.9		−57.3	−57.3	−57.4	−57.3
abh	59.8	59.8	58.9	59.9		62.6	62.6	62.7	62.8
bac	180.0	180.0	180.0	180.0	180.0	−64.1	−64.1	−64.1	−61.8

[a] Refer to Figure 1. [b] a denotes a bond length in Å; ab is the angle between two bonds; abc is the dihedral angle between the ab and bc planes (angles in degrees). [c] Reference 26.

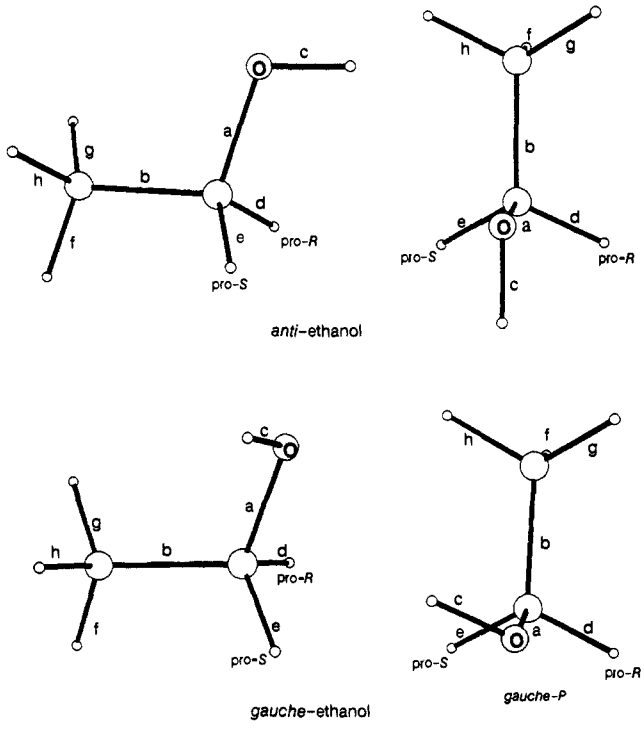

Figure 1. The structures of *anti* and *gauche* ethanol: 6-31G~ structure shown; letters are defined in Table I and are used in the definition of local symmetry coordinates (LSC) in Table IV.

of a number of compounds[25] with the most important observation being that the relative VCD intensities are unaffected by dilution; this confirms that absorption-dependent artifacts have been substantially reduced or eliminated, and supports the accuracy of CH_3CHDOH spectra measured by the same approach. The VCD spectrum in the range 800 to 1350 cm^{-1} was run on two separate occasions in CS_2 which has absorptions at each end of this window. We were unable to obtain satisfactory VCD spectra in CCl_4 which has two absorptions in the middle of this range but is clear between 1350 and 1500 cm^{-1}, owing to lack of sample.

Table II. Calculated and Relative Energies of *anti*- and *gauche*-Ethanol

	E, hartree		ΔE,
method[a]	anti	gauche	kJ/mol
SCF/6-31G*//6-1G*	−154.075 745	−154.075 575	0.45
MP2/6-31G*//6-31G*	−154.515 630	−154.515 795	−0.43
MP3/6-31G*//6-31G*	−154.541 040	−154.541 187	−0.39
MP4/6-31G*//6-31G*	−154.558 714	−154.559 031	−0.83
ZPVE SCF/6-31G*//6-31G*	225.85[b]	225.86[b]	0.01
SCF/6-31G**//6-31G**	−154.090 162	−154.090 001	0.42
MP2/6-31G**//6-31G**	−154.568 107	−154.568 241	−0.35
MP3/6-31G**//6-31G**	−154.596 513	−154.596 622	−0.29
MP4/6-31G**//6-31G**	−154.614 232	−154.614 487	−0.67
ZPVE SCF/6-31G**// 6-31G**	224.90[b]	224.95[b]	0.05
SCF/6-31+G**//6-31+G**	−154.096 040	−154.095 552	1.28
MP2/6-31+G**//6-31G**	−154.580 642	−154.580 370	0.71
MP3/6-31+G**//6-31+G**	−154.607 569	−154.607 346	0.59
MP4/6-31+G**//6-31+G**	−154.627 428	−154.627 230	0.52
ZPVE SCF/6-31+G**// 6-31+G**	224.31[b]	224.32[b]	0.01
SCF/6-31G~//6-31G~	−154.083 836	−154.083 383	1.19
ZPVE SCF/6-31G~// 6-31G~	224.42[b]	224.49[b]	0.07

[a] The notation XX/YY//ZZ means that the results cited were obtained using the theoretical method XX with basis set YY at the geometry optimized at the HF level with basis set ZZ. [b] kJ/mol.

Results and Discussion

Geometries. The 6-31G~ geometries of *anti* and *gauche* ethanol are shown in Figure 1. The former has C_s symmetry, the latter C_1. Values computed using all of the basis sets, and the experimental values (for the *anti* conformer),[26] are given in Table I. Immediately apparent from inspection of Table I is that there is no significant variation in the optimized parameters calculated using the four different basis sets, and all values are in acceptable agreement with the experimental parameters. The only significant

(25) Shaw, R. A.; Wieser, H. Unpublished results.

(26) Culot, J. P. *Austin Symp. Gas Phase Mol. Struct.* **1972**, *T8*.

Table III. Zero-Point Vibrational and Relative Energies (kJ/mol) and Populations (298 and 200 K) of Ethanol and (*S*)-*1*-*d*-Ethanol

ethanol isotopomer	ZPVE	ΔE^a	population 298 K	population 200 K
anti	224.42	0.00	0.388	0.416
gauche-P	224.49	0.59[b]	0.306	0.292
gauche-M	224.49	0.59[b]	0.306	0.292
anti-(*S*)-*1*-*d*	215.05	0.00	0.382	0.407
gauche-*P*-(*S*)-*1*-*d*	215.12	0.59	0.301	0.286
gauche-*M*-(*S*)-*1*-*d*	215.00	0.47	0.316	0.307

[a] Includes difference of 0.52 kJ/mol between Born–Oppenheimer potential energy surfaces. [b] Exp 41.2 ± 5.0 cm^{-1} (0.49 ± 0.06 kJ/mol): ref 5.

difference is the value of the COH angle which is calculated to be about 5° larger than experimental with all basis sets.

Energies. The absolute and relative energies of the *anti* and *gauche* forms obtained by the different procedures are listed in Table II. At the SCF level with all basis sets, the *anti* conformer is predicted to be more stable. Addition of electron correlation reverses this prediction *except for the largest basis set*, 6-31+G**. It is expected that the MP4/6-31+G**//6-31+G** value will be the most accurate. Therefore, for the purpose of comparing relative energies and calculating populations of deuterated isotopomers, we use the value 0.52 kJ/mol for the difference between the Born–Oppenheimer potential energy surfaces of the *anti* and *gauche* forms.

The correction to the relative energies of the *anti* and *gauche* forms due to zero-point vibrational energies (ZPVE) is predicted to be small (<0.1 kJ/mol) with all basis sets. An experimental determination of the energy difference has the *anti* conformer more stable than the *gauche* by 0.49 ± 0.06 kJ/mol.[5] Since all vibronic chiroptical properties for ethanol and its isotopomers will be calculated with the 6-31G~ basis set, values of ZPVE obtained with this basis set will be used, even though this value is slightly outside the experimental error bars. The calculated ZPVE and Boltzmann populations of ethanol and the chiral isotopomer (*S*)-*1*-deuterioethanol are presented in Table III, assuming that the calculated gas-phase result applies to dilute solution in a nonpolar solvent (CS_2 or CCl_4) and that $\Delta S = 0$. The effect of deuteration in the *pro-S* α position is to introduce a 5% bias in favor of the *gauche-M* rotamer over the *gauche-P* form. The energy differences are sufficiently small that little temperature dependence would be evident in the spectrum.

Force Field Determination

Quantum mechanical Cartesian vibrational force constants and atomic polar tensors were calculated using the 6-31G~ basis set and transformed to local symmetry coordinates (LSC) of Table IV. A set of scaling factors was transferred from 2-methyloxetane[27] to scale the force constants following the procedure of Pulay et al.,[28] providing an initial prediction of the vibrational spectra for ethanol and for the 11 deuterated isotopomers included in the experimental study of Perchard and Josien.[9] In each case, spectra were calculated for both the *gauche* and *anti* conformers, including the two distinct *gauche* conformers for each compound containing a singly deuterated methylene group. The transferred scaling factors are listed in Table IV. For each molecule the absorption spectra predicted for the *gauche* and *anti* rotamers differed sufficiently to suggest that certain experimental features might be ascribed to a single conformer. For this reason the initial assignments were limited to those cases for which corresponding transitions were predicted to coincide or were predicted with significantly different intensities. Scaling factors were then refined to fit this limited set of assignments. Factors scaling coordinates that participate only in heavily mixed normal coordinates (e.g., the CH_3 rocks) were kept fixed at the transferred values. The

Table IV. Local Symmetry Coordinates (LSC), Scale Factors, and Combined Local Symmetry Coordinates (CLSC) for Ethanol[a]

no.	LSC type	LSC definition[b]		scale factors LSC no.	scale factors transf[e]	scale factors opt[d]	CLSC[c]	CLSC ← LSC CH_3CH_2OH	CH_3CHDOH	CH_2CH_2OH	CH_3CHDOH
1	CC stretch		b	1	0.872	0.877	1	CC stretch			1
2	CO stretch		a	2	0.710	0.809	2	CO stretch			2
3	CH stretch (CH_3)		f	3, 4, 5	0.829	0.841	3	CH_3 sym stretch			3 + 4 + 5
4	CH stretch (CH_3)		g				4	CH_3 asym stretch			2(3) − 4 − 5
5	CH stretch (CH_3)		h				5	CH_2 sym stretch	CD stretch	6 + 7	6
6	CH stretch (CH_2)		e	6, 7	0.810	0.828	6	OH stretch			8
7	CH stretch (CH_2)		d				7	CH_3 sym def			9
8	OH stretch		c	8	0.795		8	CH_3 rock			10
9	CH_3 sym def	β(bf) + β(bg) + β(bh) − α(fh) − α(fg) − α(gh)		9	0.764	0.780	9	CH_3 asym def			12
10	CH_3 rock	2β(bf) − β(bg) − β(bh)		10, 11	0.806	0.809	10	CH_2 scissor	CH bend (o/p)	14	14 + 15
11	CH_3 rock	β(bg) − β(bh)					11	CH_2 wag	CD bend (o/p)	16	14 − 15
12	CH_3 asym def	2α(gh) + α(fh) − α(fg)		12, 13	0.781	0.792	12	COH bend			18
13	CH_3 asym def	α(fh) + α(fg)					13	CCO bend			19
14	CH_2 scissor	β(ad) + β(ae) + β(bd) + β(be)		14	0.767	0.792	14	CH_3 asym stretch			4–5
15	CH_2 rock	β(ad) + β(ae) + β(bd) + β(be)		15	0.808	0.871	15	CH_2 sym stretch	CH stretch	6–7	7
16	CH_2 wag	β(ad) + β(ae) + β(bd) + β(be)		16	0.757	0.786	16	CH_3 rock			11
17	CH_2 twist	β(ad) − β(ae) − β(bd) − β(be)		17	0.768	0.802	17	CH_3 asym def			13
18	COH bend	β(ac)		18	0.790	0.805	18	CH_2 rock	CH bend (i/p)	15	16 + 17
19	CCO bend	θ(ab)		19	0.832	0.899	19	CH_2 twist	CD bend (i/p)	17	16 − 17
20	OH torsion	τ(eac) + τ(dac) + τ(bac)		20			20	OH torsion			20
21	CH_3 torsion	τ(fba) + τ(gbd) + τ(hba)		20, 21	0.800	(0.800)[f]	21	CH_3 torsion			21

[a] Refer to Figure 1 for bond and angle definitions. [b] a denotes a bond length; ab is the angle between two bonds; abc is the dihedral angle between the ab and bc planes. Normalization constants are omitted. [c] Scaling factors transferred from 2-methyloxetane (ref 27). [d] Scaling factors for 6-31G~ force field of ethanol optimized to fit 202 experimental frequencies; see text. [e] For the *anti* conformer of ethanol, the first 13 CLSC transform as a′, the remainder as a″; the CLSC are used in Tables V and VI. [f] Scale factor not optimized.

(27) Shaw, R. A.; Ibrahim, N.; Wieser, H. *Can. J. Chem.* **1990**, *68*, 90–101.
(28) Pulay, P.; Fogarasi, G.; Pang, F.; Boggs, J. E. *J. Am. Chem. Soc.* **1979**, *101*, 2550–2560.
(29) Eysel, H. H.; Berlie, J. E. *J. Mol. Struct.* **1986**, *142*, 227–30.

Table V. Observed and Calculated Frequencies (cm^{-1}) and Potential Energy Distributions (PED) for Ethanol[a]

	anti rotamer						*(P)-gauche* rotamer					
	freq						freq					
no.	DLA[b]	present[c]	obs[d]	D[e]		PED[g]	DLA[b]	present[c]	obs[d]	D[e]	R[f]	PED[g]
1 A′	3687	3676	3676	52.4	6		3687	3669	(3659)	43.7	−18.9	6
2 A″	2997	2993	(2989)	55.6	14		2999	2988	(2989)	59.1	27.0	14 (60) + 4 (32)
3 A′	2988	2984	(2989)	51.8	4		2976	2971	(2989)	87.6	−146.6	4 (54) + 15 (22) + 14 (13)
4 A′	2924	2924	(2928)	24.1	3		2917	2910	(2901)	23.6	−4.9	3
5 A″	2910	2901	(2901)	71.5	15		2926	2950	(2989)	7.0	126.7	15 (44) + 14 (23) + 5 (17)
6 A′	2886	2877	(2901)	85.0	5		2891	2887	(2901)	81.9	8.0	5 (71) + 15 (22)
7 A′	1486	1488	1480	3.6	10		1482	1482	(1480)	1.2	11.2	10
8 A′	1457	1459	(1450)	7.0	9		1451	1455	1450	4.1	1.0	9
9 A″	1440	1444	1450	13.3	17		1443	1449	1450	15.2	−10.8	17
10 A′	1430	1422	(1450)	38.2	11 (61) + 1 (16) + 12 (14)		1401	1389	1394	122.1	−171.6	11 (50) + 7 (34) + 1 (15)
11 A′	1372	1364		1.2	7 (87) + 11 (14)		1372	1365	1370	41.5	106.8	7 (58) + 12 (14) + 11 (14)
12 A″	1262	1272		0.2	19 (72) + 16 (14)		1249	1262	1251	23.3	−464.7	19 (41) + 16 (21) + 18 (14)
13 A′	1243	1245	1241	274.2	12 (54) + 11 (18) + 8 (12)		1033	1050	(1058)	58.5	414.8	12 (29) + 1 (25) + 8 (16)
14 A″	1150	1184		17.6	18 (53) + 16 (20) + 19 (14)		1345	1341		15.2	−32.2	11 (35) + 19 (23) + 12 (20)
15 A′	1064	1082	1089	97.8	2 (54) + 8 (19)		1105	1123		19.0	−127.1	8 (26) + 18 (15) + 13 (14)
16 A′	1010	1031	1038	219.6	1 (44) + 12 (26) + 8 (19)		1058	1068	1066	427.3	335.2	2 (59) + 1 (24) + 12 (14)
17 A′	867	884	892	65.9	2 (39) + 1 (29) + 8 (29)		863	874	879	72.6	10.9	2 (36) + 1 (31) + 8 (29)
18 A″	787	814	(801)	0.2	16 (62) + 18 (49) + 19 (17)		774	799	801	11.2	−43.8	16 (58) + 18 (53) + 19 (15)
19 A′	398	418	419	108.7	13 (135) + 10 (51) + 8 (21)		418	422	419	91.8	44.6	13 (143) + 10 (62) + 8 (22)
20 A″	293	265		1316.2	20 (72) + 21 (17)		303	269		1507.3	570.6	20 (79) + 21 (21)
21 A″	255	227		688.1	21 (86) + 20 (30)		262	243		415.9	−708.4	21 (78) + 20 (20)

[a] 6-31G~ basis set and geometry. [b] Reference 14; 6-31G** basis; scaled force field. [c] Present work; frequencies and positions calculated using optimized scaling factors of Table IV. Transitions are paired with the most similar normal coordinates of the *anti* rotamer: see text. [d] Frequencies in parentheses were not used in the optimization of scaling factors. [e] esu^2 cm^2 × 10^{40}. [f] esu^2 cm^2 × 10^{45}. [g] PED in combined local symmetry coordinates (CLSC) for CH_3CH_2OH (Table IV); numbers in parentheses are the diagonal coefficients (×100) of the PED. CLSCs with coefficients larger than 0.1, or the three with the largest coefficients, are listed; where no number appears, that CLSC has a coefficient >0.8 in the PED.

Table VI. Observed and Calculated Frequencies (cm^{-1}) and Potential Energy Distributions (PED) for *1-d*-Ethanol[a]

	anti rotamer			*(P)-gauche* rotamer			*(M)-gauche* rotamer		
no.	calc	obs[b]	PED[c]	calc	obs[b]	PED[c]	calc	obs[b]	PED[c]
1	3676	(3676)	6	3669	(3659)	6	3669	(3659)	6
2	2992	(2985)	14	2987	(2981)	14 (60) + 4 (37)	2987	(2981)	14 (56) + 4 (42)
3	2984	(2977)	4	2971	(2971)	4 (51) + 15 (29) + 14 (20)	2964	(2967)	4 (59) + 14 (40)
4	2924	(2943)	3	2910	(2896)	3	2911	(2896)	3
5	2889	(2896)	15	2949	(2943)	15 (69) + 14 (17) + 4 (14)	2891	(2896)	15
6	2125	(2145)	5	2126	(2145)	5	2176	(2171)	5
7	1459	1461	9	1456	1461	9	1457	1461	9
8	1444	1444	17	1448	1444	17	1448	1444	17
9	1397	1384	7 (43) + 18 (25) + 1 (23)	1383	1380	7 (39) + 18 (33) + 1 (12)	1376	(1380)	7 (89) + 1 (15)
10	1354	(1348)	7 (53) + 18 (20) + 12 (10)	1332	(1332)	10 (43) + 18 (19)	1330	(1332)	18 (75) + 7 (10)
11	1351	(1348)	10 (53) + 18 (17)	1368	(1380)	7 (55) + 10 (18) + 18 (12)	1369	(1380)	10 (49) + 12 (17)
12	1249	1251	12 (43) + 18 (21) + 10 (11)	1065	(1061)	8 (37) + 1 (22) + 12 (15)	1252	1251	12 (63) + 11 (14)
13	1142	1140	16 (25) + 2 (21) + 19 (18)	1145	1140	19 (26) + 16 (24) + 2 (23)	1145	1140	16 (34) + 19 (20) + 1 (20)
14	1101	(1107)	2 (23) + 11 (22) + 16 (15)	1271	(1251)	12 (37) + 18 (23)	1117	1107	8 (36) + 2 (31) + 13 (15)
15	1024	1021	1 (39) + 8 (21) + 12 (21)	1049	1047	2 (34) + 16 (21) + 12 (17)	1037	(1047)	1 (31) + 2 (20) + 16 (13)
16	926	940	19 (42) + 2 (26) + 11 (20)	922	(917)	19 (37) + 2 (25) + 11 (18)	906	917	19 (39) + 2 (28) + 11 (16)
17	872	879	1 (29) + 8 (27) + 2 (23)	858	863	1 (32) + 8 (24) + 2 (19)	859	(863)	1 (28) + 8 (27) + 19 (19)
18	727	717	11 (67) + 10 (43) + 16 (42)	717	717	11 (75) + 10 (51) + 16 (41)	715	717	11 (77) + 10 (50) + 16 (41)
19	415	427	13 (135) + 11 (21) + 8 (21)	419	427	13 (143) + 11 (29) + 8 (23)	418	427	13 (143) + 8 (22) + 11 (22)
20	264		20 (75) + 21 (15)	266		20 (84) + 21 (16)	266		20 (84) + 21 (16)
21	226		21 (89) + 70 (17)	242		21 (84) + 20 (15)	244		21 (84) + 20 (15)

[a] Frequencies and positions calculated using optimized scaling factors of Table IV. [b] Frequencies in parentheses were not used in the optimization of scaling factors. [c] PED in combined local symmetry coordinates (CLSC) for CH_3CHDOH (Table IV); numbers in parentheses are the diagonal coefficients (×100) of the PED. CLSCs with coefficients larger than 0.1, or the three with the largest coefficients, are listed; where no number appears, that CLSC has a coefficient >0.8 in the PED.

new set of adjusted frequencies and intensities was then used to secure a total of 202 assignments, and all scaling factors except the two torsions were then refined to fit the vapor-phase positions.[9] The optimized scaling factors are listed in Table IV. The vibrational assignments are listed in Tables V and VI for ethanol and *1-d*-ethanol, respectively. The LSCs are combined to form the CLSCs of Table IV; it is these coordinates that are used in determining the potential energy distribution (PED) of Tables V and VI. Note that these coordinates differ for ethanol and *1-d*-ethanol; for *anti* ethanol each is full symmetry coordinate, *A′* or *A″*, while for *1-d*-ethanol, the natural coordinates separate the CH from the CD modes of the CHD group. The unusual definition for the CH_2 scissoring coordinate (LSC no. 14) was chosen to permit subsequent "unsymmetrization" of the CH_2 bends (see CLSC nos. 10 and 11). This leads to the minor disadvantage of a very large coupling force constant between the CH_2 scissor and CCO bend, and hence to the unusually large diagonal PED elements for the CCO bend (ν_{19}) in Tables V and VI. A complete listing of the calculated and assigned transitions for all deuterated species is available from the authors upon request. For the present purpose, we list in Table V the results for the *anti* and *gauche* isomers of ethanol (undeuterated), and in Table VI the results for the *anti* and two *gauche* isomers of *1-d*-ethanol. The calculated frequencies of Dothe, Lowe, and Alper (DLA)[14] who obtained their force field by scaling a 6-31G** force field against the same data of Perchard and Josien[9] are also reproduced in Table VI. Our procedure differs in a number of important respects from that of DLA. We used the same scale factor for each of the two methylene stretches, rather than independent factors for each C–H in each conformer, trusting that the ab initio force field will

Table VII. Calculated Frequencies (cm^{-1}), Dipole Strenghts, Optical Rotatory Strengths, and Normal Mode Mixing for (*S*)-*1*-*d*-Ethanol[a]

	anti rotamer			(*P*)-*gauche* rotamer				(*M*)-*gauche* rotamer			
no.	ν_{calc}, cm^{-1}	D_{calc},[b] esu^2 cm^2	R_{calc},[c] esu^2 cm^2	ν_{calc}, cm^{-1}	D_{calc},[b] esu^2 cm^2	R_{calc},[c] esu^2 cm^2	PED[d]	ν_{calc}, cm^{-1}	D_{calc},[b] esu^2 cm^2	R_{calc},[c] esu^2 cm^2	PED[d]
1	3676	52.5	−0.7	3669	43.7	−17.2	1	3669	44.5	19.4	1
2	2992	47.5	30.8	2987	42.9	5.0	2 (56) + 3 (42)	2987	52.8	53.7	2 (61) + 3 (38)
3	2984	47.8	−27.8	2971	91.1	−70.4	3 (49) + 2 (28) + 5 (20)	2964	54.1	−48.9	3 (61) + 2 (35)
4	2924	24.8	−21.0	2910	26.8	1.4	4	2911	27.0	−11.7	4
5	2889	78.8	−4.9	2949	8.9	40.7	5 (79) + 2 (12)	2891	77.4	−51.2	5
6	2125	76.4	−0.1	2126	76.6	39.5	6	2176	39.9	39.9	6
7	1459	4.8	−6.0	1456	6.2	−7.8	7	1457	7.7	−12.3	7
8	1444	14.1	15.6	1448	15.1	−6.8	8	1448	14.7	−8.1	8
9	1397	18.3	−20.1	1383	123.3	−196.4	9 (36) + 12 (20) + 10 (12)	1376	29.3	35.8	9 (69) + 10 (25)
10	1354	10.2	−114.6	1332	9.9	213.4	10 (43) + 11 (27) + 12 (16)	1330	33.1	325.7	10 (58) + 12 (24) + 9 (13)
11	1351	15.6	−100.2	1368	24.5	3.5	11 (38) + 9 (26) + 10 (17)	1369	19.1	103.3	11
12	1249	187.3	814.4	1065	95.6	409.2	12 (43) + 15 (30) + 9 (11)	1252	268.6	92.2	12 (25) + 15 (22) + 11 (14)
13	1142	162.1	−741.0	1145	97.4	−520.0	13	1145	76.2	−460.9	13
14	1101	26.6	−75.2	1271	24.1	−227.1	14 (29) + 11 (20) + 9 (20)	1117	94.8	26.2	14 (60) + 15 (21)
15	1024	209.0	193.2	1049	324.4	503.2	15 (50) + 14 (56)	1037	21.1	−34.7	15 (55) + 14 (24) + 12 (12)
16	926	20.0	75.4	922	11.8	−107.0	16	906	229.9	−99.3	16
17	872	48.9	−5.2	858	70.3	−14.7	17	859	4.7	−11.2	17
18	727	2.4	34.4	717	9.4	−52.6	18	715	13.0	87.1	18
19	415	106.5	−27.9	419	91.9	45.4	19	418	89.3	−39.0	19
20	264	1402.6	−8.4	266	1607.7	581.9	20	266	1616.1	−586.5	20
21	226	603.2	−14.5	242	312.9	−649.2	21	244	314.7	653.9	21

[a] Frequencies calculated using optimized scaling factors of Table IV; 6-31G~ basis set used for dipole and rotatory strengths. [b] $\times 10^{40}$. [c] $\times 10^{45}$. [d] PED in normal coordinates of the *anti* rotamer (see text); numbers in parentheses are the diagonal coefficients (×100) of the PED. Normal coordinates with coefficients larger than 0.1, or the three with the largest coefficients, are listed; where no number appears, that normal mode has a coefficient >0.8 in the PED with no other contribution >0.1.

correctly reflect the intrinsic environmental differences of the C–H bonds in the two rotamers. DLA used the same set of observed frequencies for both *anti* and *gauche* forms, whereas our procedure allows more precise assignments to be made. Some of these are discussed below.

The ordering of the transitions listed in Table V for the *gauche* isomer and in Table VI for the two *gauche* isomers was determined by matching the normal coordinates in each case to the *most similar* coordinate of the *anti* conformer. The similarity is made quantitative by a transformation involving the eigenvectors of the Wilson FG matrix (in local symmetry coordinates (LSC)) of the *gauche* and *anti* forms, $\mathbf{L}_{gauche}$ and $\mathbf{L}_{anti}$, respectively.[27] Specifically, the column vectors of the matrix product, $\mathbf{L}_{anti}^{-1}\mathbf{L}_{gauche}$, give the normal coordinates of the *gauche* conformer as a linear combination of those of the *anti* species, as indicated by the relationship

$$Q_{anti} = \mathbf{L}_{anti}^{-1}\mathbf{L}_{gauche}Q_{gauche}$$

The jth element of the ith column of $\mathbf{L}_{anti}^{-1}\mathbf{L}_{gauche}$ gives a measure of the similarity of the jth normal coordinate of the *anti* form to the ith normal mode of the *gauche* form. The potential energy distribution (PED) of the ith normal mode of the *gauche* form, in terms of contributions from the normal coordinates of the *anti* form, is

$$\mathrm{PED}^{i}_{gauche} = \sum_{j}(\mathbf{L}_{anti}^{-1}\mathbf{L}_{gauche})_{ji}(\mathbf{L}_{anti}^{T}\mathbf{F}_{gauche}\mathbf{L}_{anti})_{jj}/\lambda_i$$

Table VII lists the vibrational assignments for the two *gauche* conformers of (*S*)-*1*-*d*-ethanol as determined by this analysis; the elements of the PED matrix express the mixing of the *anti* normal coordinates that occurs for each of the *gauche* species. This kind of *similarity* analysis may prove useful for understanding the origin of intensity in the calculated IR and VCD spectra, specifically in rationalizing correlations or differences among spectra of structurally similar molecules.

IR Spectra

Ethanol. Dipole strengths were evaluated at the 6-31G~ equilibrium geometry and using the vibronic coupling formalism of Nafie and Freedman[12] (formally equivalent to atomic polar tensor (APT) theory for the electric dipole strengths) and 6-31G~ wave functions. The dipole strengths are listed in Table V. The calculated IR spectra in the range 800–1500 cm^{-1} of *anti* and *gauche* ethanol and of the *predicted* equilibrium mixture at 298 K together with the experimental solution spectrum are plotted in Figure 2. The agreement between the calculated and experimental spectra is very satisfactory. The dilute solution spectrum features a strong absorption at 1058 cm^{-1} flanked by distinct shoulders at 1031 and 1082 cm^{-1}. The calculated spectrum has a prominent absorption at 1050 cm^{-1} which originates in the *gauche* conformers. The *anti* conformer has two transitions in

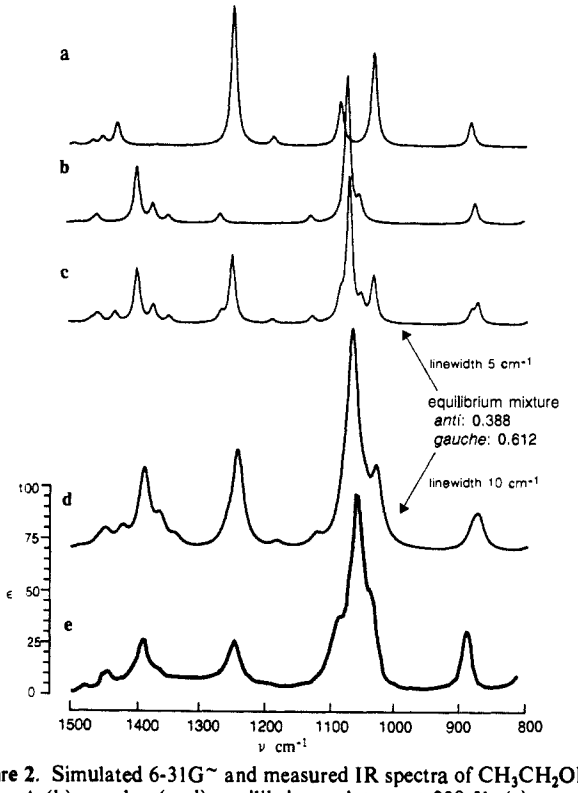

Figure 2. Simulated 6-31G~ and measured IR spectra of CH_3CH_2OH: (a) *anti*; (b) gauche; (c, d) equilibrium mixture at 298 K; (e) experimental spectrum, 0.08 M in CCl_4, 1-mm path. For a, b, c, the line width at half-height is 5 cm^{-1} (for clarity) and the molar absorptivity scale is 4.5 times that shown for the experimental spectrum e. For d, the line width is 10 cm^{-1} and the ϵ scale is the same as for the experimental spectrum e.

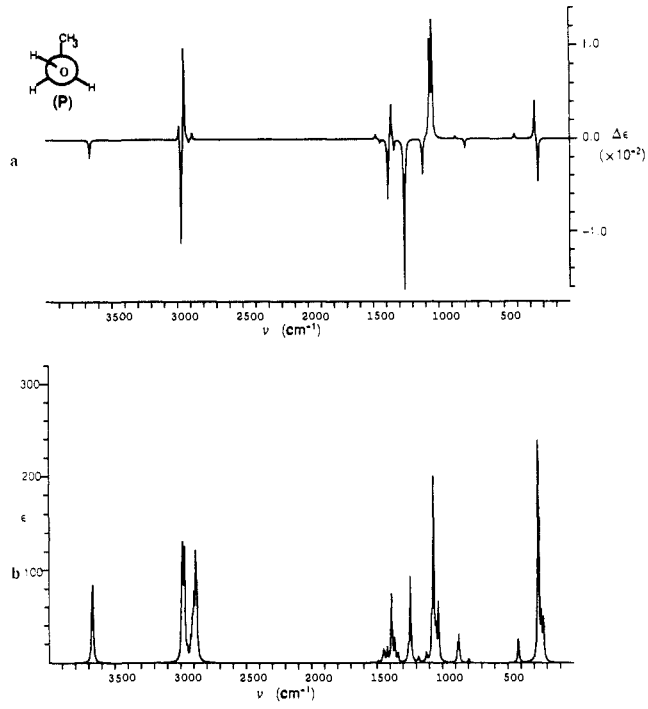

Figure 3. (a) Simulated VCD spectrum of (*P*)-*gauche*-ethanol; 6-31G~ scaled force field and vibronic coupling theory; (b) simulated IR spectrum of undeuterated ethanol (equilibrium mixture).

this region, at 1010 and 1064 cm^{-1}. In the simulated spectrum (Figure 2), the latter is not resolved. However, it is likely that the 1031 and 1082 shoulders in the observed spectrum originate in the *anti* form. The discrepancy in relative positions probably results from our choice in refining to vapor phase as opposed to solution positions. The peak observed at 1241 cm^{-1} is also due to the *anti* conformer (calc 1245 cm^{-1}). That observed at 880 cm^{-1} is calculated to be of equal intensity and at nearly the same frequency in both conformers. A number of weak absorptions are expected from both rotamers in the 1300- to 1500-cm^{-1} range. The most prominent of these originates in the *gauche* form at 1388 cm^{-1} (obs 1380 cm^{-1}).

The complete simulated IR spectrum of undeuterated ethanol (and the VCD spectrum of the (*P*)-*gauche* conformer) is shown in Figure 3.

***1-d*-Ethanol.** The experimental IR and VCD spectra in the 800- to 1500-cm^{-1} range are shown in Figure 4, together with the simulated 298 K calculated spectra. The overall similarity of the experimental and calculated spectra is striking. The calculated dipole strengths of absorptions at 1100 and 1250 cm^{-1} are underestimated and overestimated, respectively, to some extent compared to experiment, which leads to a similar effect on the rotatory strengths. We reserve discussion of the latter to later sections.

The calculated individual components and averaged IR spectra of *1-d*-ethanol are displayed in Figure 5. Some features of the composite spectrum, which closely resembles the observed spectrum (Figure 4), are clearly attributable to individual components of the equilibrium mixture. The peak near 910 cm^{-1} (obs 917 cm^{-1}) originates from the (*M*)-*gauche* conformer, the equivalent normal mode of neither of the other two conformers having significant intensity in this region. The calculated peak at 1024 cm^{-1} which is observed as a shoulder at 1021 cm^{-1} is predicted to originate from the *anti* conformation. The more prominent peak observed at 1047 cm^{-1} arises from a complex mode of the (*P*)-*gauche* rotamer. The peak at 1107 cm^{-1} in the experimental spectrum corresponds to the relatively weaker transition predicted to occur at 1117 cm^{-1} in the (*M*)-*gauche* isomer. Evidently the intensity of this peak (and/or the peak at 1101 cm^{-1} in the *anti* form) is underestimated by the calculation. The adjacent strong feature observed at 1140 cm^{-1} is a superposition of a moderate strength absorption occurring in each of the three conformers.

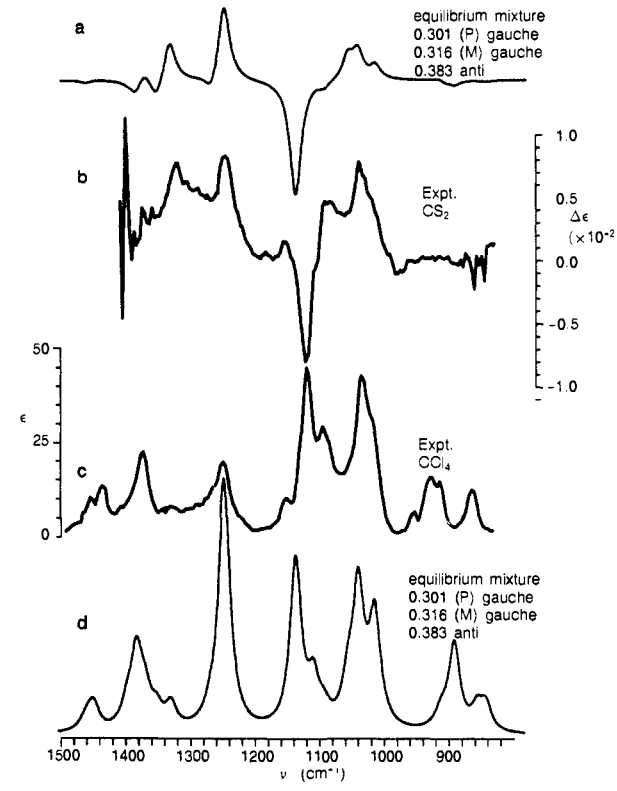

Figure 4. IR and VCD spectra of (*S*)-*1-d*-ethanol: (a) simulated VCD spectrum of the equilibrium mixture at 298 K, 6-31G~ basis set, scaled quantum mechanical force field; (b) VCD exp 0.13 M in CS_2, 1-mm path, 40000 VCD scans; (c) IR exp 0.13 M in CCl_4, 1-mm path; (d) simulated IR spectrum of the equilibrium mixture at 298 K. Simulated spectra are on the same scale as the experimental spectra and have line width at half-height 10 cm^{-1}.

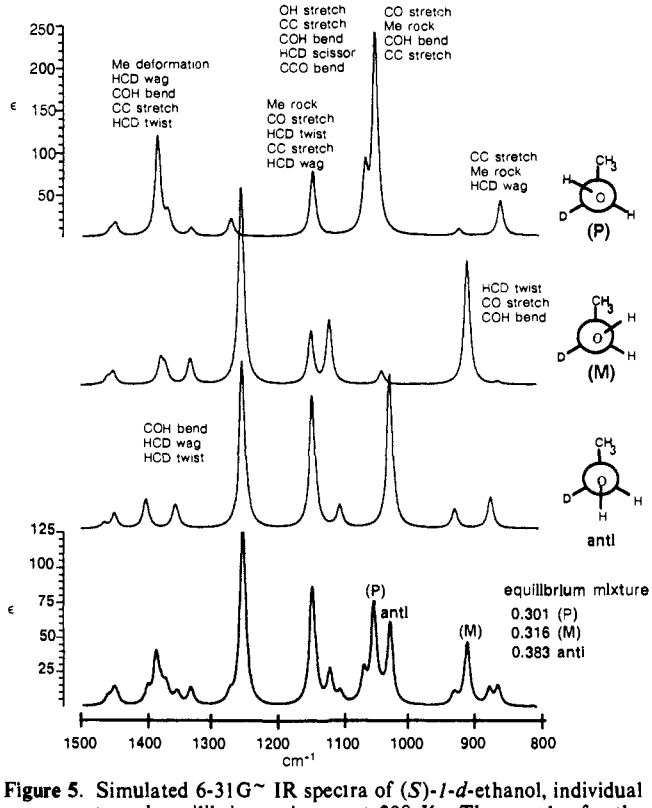

Figure 5. Simulated 6-31G~ IR spectra of (*S*)-*1-d*-ethanol, individual components and equilibrium mixture at 298 K. The ε scales for the components are the same as shown for (*P*).

The moderately strong peak observed at 1251 cm^{-1} is predicted to be strong in both the *anti* and (*M*)-*gauche* isomers, but not the (*P*)-*gauche* species. The mode, which, according to the analysis

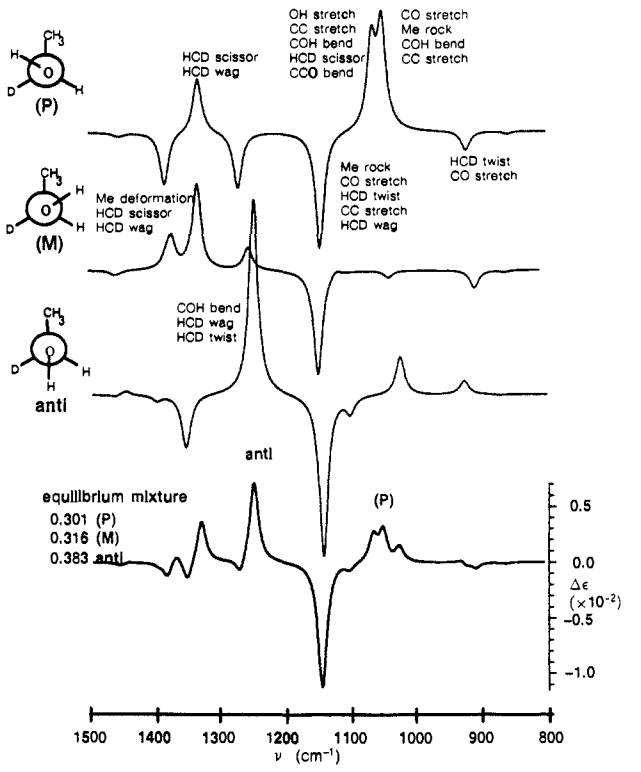

Figure 6. Simulated 6-31G~ VCD spectra of (*S*)-*1*-*d*-ethanol, individual components and equilibrium mixture at 298 K. The vertical scale is the same for all spectra.

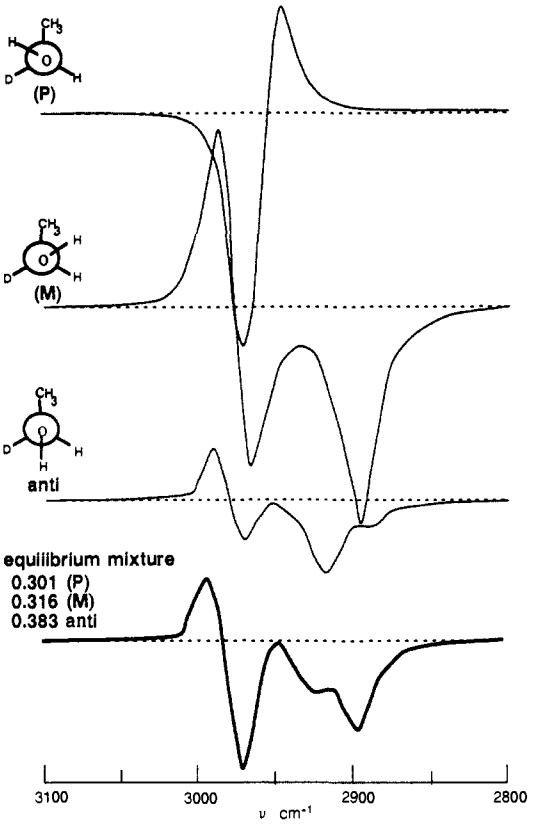

Figure 7. Simulated VCD spectra of (*S*)-*1*-*d*-ethanol in the CH stretching region.

of Table VI, is dominated by CLSC 12, the COH bend (Table IV), mixed with an α-CH bend, ultimately reflects the *gauche* orientation of the OH and CH bonds unique to the *anti* and (*M*)-*gauche* conformers. The reason that the calculated intensity for this mode is too large is uncertain, particularly in view of the good agreement in the corresponding transition (1241 cm^{-1}) of the parent compound. It is possible that mixing of this and the weak (calculated) mode at 1117 cm^{-1} in the (*M*)-*gauche* isomer is incorrect since these modes are calculated to be closer in frequency than actually observed and that this has the consequence of redistributing the intensity toward the higher frequency peak. This explanation seems unlikely, however, since the PED analyses of Tables VI and VII show no commonalty for the two absorptions which are only weakly coupled.

VCD Spectra

(*P*)-*gauche*-Ethanol. The simulated VCD spectrum of the *gauche* isomer of (*P*) chirality is shown in Figure 3. The calculated rotatory strengths are listed in Table V. Strong Cotton effects (CE) are predicted in the C–H stretching region and in the mid-IR. Ethanol is optically inactive because the mirror image VCD spectra of the two *gauche* conformers exactly cancel. On the other hand, the two *gauche* conformers of α-*d* ethanol are not of the same energy, and many of the spectral absorptions are calculated to occur in different regions of the spectrum. Under these circumstances the VCD spectrum of the undeuterated species serves as a template for VCD features expected from intrinsic skeletal chirality, as opposed to the more local chirality due to introduction of a D in place of H. The spectrum is dominated by the two strong positive CEs and the single negative CE at 1050, 1068, and 1262 cm^{-1}, respectively. The COH bend features in all three modes, mixed to different extents with Me rock, CH_2 twist, and CC stretching motions.

(*S*)-α-*d*-Ethanol. The simulated VCD spectrum of (*S*)-*1*-*d*-ethanol and the observed VCD spectrum are displayed in Figure 4 in the 800–1500-cm^{-1} region. The main features of the experimental spectrum are very well reproduced in the simulation. An analysis of the theoretical VCD of the individual components of the equilibrium mixture is presented in Figure 6. The strong negative feature at 1120 cm^{-1} in the experimental spectrum originates from each component of the equilibrium mixture. The mode is very complex, being a mixture of Me rocking, CO and CC stretching, and CHD twist–wag motions. Other features of the experimental spectrum are clearly identifiable as originating from separate components. The strong positive CE at 1250 cm^{-1} arises from the predominantly COH bending mode of the *anti* conformer, there being only weak CD from the two *gauche* forms in this region. The positive CD between 1030 and 1100 cm^{-1} is predicted to originate in the main from the (*P*)-*gauche* conformer with perhaps a small component from the *anti* form. Both *gauche* forms contribute to the positive CD at 1310 cm^{-1} but not the *anti* which is predicted to have a negative CD in this region.

The simulated VCD spectrum of (*S*)-*1*-*d*-ethanol in the CH stretching region and the spectra of the three rotamers are shown in Figure 7. Comparison with the spectra of Pultz[11] (who measured the (*R*) enantiomer) reveals broad agreement. Interpreting Pultz's VCD spectrum in terms of the (*S*) enantiomer, the VCD signal spans the range 2850 to 3000 cm^{-1} and is negative throughout the range except for a relatively weak positive CE at 2980 cm^{-1}. The negative CE maximum at 2900 cm^{-1} and negative CE shoulder at 2920 cm^{-1} match very well the results of the present calculation (Figure 7). However, Pultz's spectrum does not display the almost zero ΔA near 2950 cm^{-1}, and it is clear that the negative band at 2970 cm^{-1} is exaggerated in the present work. Inspection of the individual components plotted in Figure 7 reveals that the VCD spectrum in the CH region arises mainly from the (*M*)–(*S*) diastereomer to which the net positive CE near 3000 cm^{-1} and the negative peak at 2900 cm^{-1} may be attributed.

The VCD features intuitively may be expected to fall into two categories, either reflecting the chirality of the CHD center or the handedness (*P* or *M*) of the CCOH torsional angle. The technique described above in the Force Field Determination section for establishing the resemblance among normal coordinates of the three conformers may be used to identify modes that are either (i) unaffected by changes in the OH torsion angle or (ii) unaffected by the interchange of H and D at the chiral center. Inspection of Table VII reveals several instances where the normal coordinates of the two *gauche* species comprise essentially the same set of LSC

Table VIII. Comparison of VCD Intensities of (*S*)-*1-d*-Ethanol by the Vibronic Coupling Theory (VC) and Stephens' Formalism (PJS)

anti			*P-gauche*			*M-gauche*		
freq[a]	*R*(VC)[b]	*R*(PJS)[c]	freq[a]	*R*(VC)[b]	*R*(PJS)[c]	freq[a]	*R*(VC)[b]	*R*(PJS)[c]
225.7	−14.5		242.3	−649.2		242.3	653.9	
264.0	−8.4		265.9	581.9		266.4	−586.5	
415.4	−27.9		418.8	45.4		418.3	−39.0	
727.1	34.4		716.7	−52.6		715.1	87.1	
871.8	−5.2		858.5	−14.7		859.3	−11.2	
926.1	75.4		921.7	−107.0		905.6	−99.3	
1024.0	193.2		1048.9	503.2		1036.6	−34.7	
1100.6	−75.2		1064.4	409.2		1116.5	26.2	
1141.1	−741.0		1144.7	−520.0		1144.5	−460.9	
1248.7	814.4		1270.4	−227.1		1251.1	92.2	
1350.1	−100.2	−112	1331.2	213.4	13	1329.8	325.7	110
1353.2	−114.6	16	1367.2	3.5	−82	1368.1	103.3	27
1396.2	−20.1	9.2	1382.6	−196.4	−62	1375.3	35.8	11
1443.6	15.6		1447.9	−6.8		1447.8	−8.1	
1459.1	−6.0		1455.7	−7.8		1456.4	−12.3	
2125.6	−0.1	−5.8	2126.8	39.5	36	2176.2	39.9	−13
2889.2	−4.9	26	2910.2	1.4	18	2890.7	−51.2	−139
2923.7	−21.0	−28	2948.3	40.7	7.2	2911.1	−11.7	90
2983.5	−27.8	−45	2970.4	−70.4	24	2963.8	−48.9	−15
2992.1	30.8	53	2986.4	5.0	−43	2987.0	53.7	65
3675.8	−0.7		3668.4	−17.2		3668.3	19.4	

[a] Present results; units cm^{-1}. [b] Present results; units: *D*, $esu^2\ cm^2 \times 10^{-40}$; *R*, $esu^2\ cm^2 \times 10^{-45}$; Vibronic coupling theory, 6-31G~ basis set. [c] Reference 14. The signs are reversed to coincide with the (*S*) enantiomer, *P* corresponds to *gauche*-B″, *M* corresponds to *gauche*-A″; Stephens' theory, 6-31G* basis set.

displacements as the corresponding mode of the *anti* rotamer. The implications of these cases on the VCD spectra are as follows. We notice that the CH stretching modes do change significantly when the OH group is rotated. The two most striking effects are the rearrangement of the near-degenerate pair of CH_3 asymmetric stretches, ν_2 and ν_3, and the 60-cm^{-1} upward shift in the position of the C*H stretch of the (*P*)-*gauche* rotamer relative to the other two species. The C*H stretch also mixes with the lower wavenumber CH_3 asymmetric stretch for the (*P*)-*gauche* rotamer. Given these changes in the normal modes, it is not surprising that little correlation apparently exists among the three calculated CH stretching VCD spectra (Table VII and Figure 7); the consistency in sign for ν_3 is probably coincidental. The clearest examples of VCD that reflect the conformation of the OH almost exclusively are the OH stretch and the two torsions, ν_{20} and ν_{21}. This is confirmed by comparing the normal coordinates of two *gauche* diastereomers having the same OH configuration but with the sites of deuterium substitution interchanged, i.e., (*P*)-(*S*) and (*P*)-(*R*). This comparison (details not shown) indicates that each of the three modes cited is essentially unaffected by interchanging H and D, and hence that the normal modes of the two *gauche* forms of the (*S*)-*1-d* system are mirror images. The same behavior is also indicated for ν_{18} and ν_{19}. All of these modes, ν_1 and ν_{18}–ν_{21}, thus would be expected to provide nearly equal and opposite VCD signals for the two *gauche* rotamers, reflecting the mirror image relation between the corresponding normal coordinates. The calculated rotatory strengths (Table VII) are uniformly in accord with this indication. Further evidence supporting the argument that the configuration of the CHD moiety is unimportant in these modes is found in observing that calculated rotatory strengths for (*P*)-*gauche*-ethanol (Table V) are invariably of the same sign and order-of-magnitude intensity as for the corresponding modes (ν_1, ν_{18}–ν_{21}) of (*P*)-*gauche*-(*S*)-*1-d*-ethanol.

There are several other modes for which the LSC displacements remain very similar for the rotamers of (*S*)-*1-d*-ethanol, including ν_6 (CD stretch), ν_{13}, ν_{16}, and ν_{17}. These are distinguished from the vibrations discussed above by the fact that each involves significant participation of the CHD stretches or deformations. These normal coordinates of the two *gauche* conformers are *not* mirror images (as verified using the technique described above for comparing the vibrational modes of species identical except for the interchange of H and D) and hence would be expected to provide VCD bands reflecting the absolute configuration of the CHD group. This is indeed the case for the calculated rotatory strengths for each pair of matching transitions of the two *gauche* conformers (see Table VII). For ν_6 and ν_{16} the normal coordinates evidently include some participation of the OH group, and the correlation does not extend to the *anti* conformer. For both ν_{13} and ν_{17} the normal coordinates are nearly identical for all three rotamers and do not include participation of the OH group. This indicates that the clearest configurational marker band, predicted with strong negative intensity in all VCD spectra at 1142–1145 cm^{-1} (see Figure 6), does not result from coincidental matching of the positions and calculated intensities but rather from the close similarity of this rather complex mode in the three rotamers. Small wonder then that the corresponding experimental feature (Figure 4) is the most prominent in the 800–1500-cm^{-1} range.

Comparison of Vibronic Coupling VCD to VCD by Stephens' Method

Optically active α-deuterioethanol provides an opportunity for comparison of results calculated by Stephens' formalism[15] and the vibronic coupling theory[12] to each other and to experiment. Dothe, Lowe, and Alper (DLA)[14] have reported VCD and IR intensities for ethanol and all deuterated isotopomers, calculated using Stephens' method, scaled quantum mechanical force fields evaluated by numerical differentiation, and the 6-31G* basis set. Polar and axial tensors were evaluated at the distributed origin gauge[30] and a common origin (center of mass) gauge. The distributed origin results, which were deemed to be more reliable, are reproduced in Table VIII for both *gauche* rotamers and for the *anti* form. The data in Table VIII have the signs reversed to correspond to the (*S*) enantiomer. The present vibronic coupling results are reproduced in Table VIII for ease of comparison. DLA had available the VCD results of Pultz[11] who measured the VCD of (*R*)-*1-d*-ethanol and (*R*)-*1*,*O*-d_2-ethanol in the C–H stretching region, and of the latter in the mid-IR region. By attributing the dominant features of the experimental spectrum *entirely* to an equimixture of the two *gauche* conformers, DLA also found substantial agreement with the observed pattern of signs except for the band at 2930 cm^{-1} attributed to the symmetric methyl deformation for which they obtained the opposite sign.

The results of DLA agree in the main with the present results in sign (Table VIII). Absolute intensities are very different, in some cases by more than an order of magnitude. The origin of the differences is not certain. In the Stephens' method results of DLA, origin dependence of the magnetic dipole transition

(30) Jalkanen, K. J.; Stephens, P. J.; Amos, R. D.; Handy, N. C. *J. Phys. Chem.* **1988**, *92*, 1781.

moment has been eliminated by use of the distributed origin gauge. However, the basis set, though large, does not have the extensive polarization which Stephens' investigations on NHDT[30,31] suggest is necessary for converged results. On the other hand, the present results were obtained with a very large (equivalent in size to 6-311G**), properly derivatized, basis set, but were evaluated in the common origin gauge (center of mass) and are origin dependent. The agreement between calculated and experimental spectra suggests that the present results are not far from the correct values. More comparisons are necessary before one could conclude that the center of mass is a reasonable choice of origin and/or that the origin dependence is not severe with the 6-31G~ basis set.

(31) (a) Jalkanen, K. J.; Stephens, P. J.; Lazzeretti, P.; Zanasi, R. *J. Chem. Phys.* **1989**, *90*, 3204-3213. (b) Jalkanen, K. J.; Stephens, P. J.; Amos, R. D.; Handy, N. C. *Chem. Phys. Lett.* **1987**, *142*, 153-158.

Acknowledgment. The authors are grateful to Professors H. S. Mosher and T. Cronholm who kindly provided samples of optically active α-*d*-ethanol from which the measured VCD spectra were obtained. The financial support of the Natural Sciences and Engineering Research Council of Canada is gratefully acknowledged. We also thank Supercomputer Services of the University of Calgary for generous allocations of CPU time on the CDC Cyber 205.

Theoretical Study of Ethylene–Noble Metal Complexes

G. Nicolas* and F. Spiegelmann

Contribution from the Laboratoire de Physique Quantique, U.A. 505 du CNRS Université Paul Sabatier, 118, Route de Narbonne, 31062 Toulouse Cedex, France. *Received July 14, 1989*

Abstract: The interaction of ethylene with copper, silver, or gold atoms is investigated through theoretical calculations, including electron correlation effects. The $d^{10}s^1$ atomic configuration of the three metals gives rise to a weakly bound $^2A_1$ ground state ($D_e < 12$ kcal·mol^{-1}) in which the interaction is analyzed as a van der Waals one. The $^2B_1$ and $^2B_2$ states arising from the $d^{10}p^1$ atomic configurations give more bound complexes ($D_e > 20$ kcal·mol^{-1}). Gold is found to have the highest complexing ability, while silver yields the less bound complexes. The calculated vertical transitions are in good agreement with the observed UV-visible spectrum of CuC_2H_4 and AuC_2H_4. These transitions are related to s → p excitations of the metal unpaired electron.

I. Introduction

In recent years, low-temperature cocondensation of metal atoms with alkenes[1] or alkynes[2] in rare-gas matrices has provided various spectroscopic data such as infrared (IR) and Raman vibrationnal spectra,[3,4] UV-visible absorption spectra,[5-9] and electron spin resonance (ESR) studies.[10-14]

This is the case for copper, silver, and gold metal atoms M, which have been observed to react with ethylene and form $M_n(C_2H_4)_m$ complexes. However, the numerous experimental data available on this series reveal some contradictions. Indeed, the ESR experiments of Kasai et al.[15,16] give evidence for the biligand $M(C_2H_4)_2$ complexes with the three metals, while the monoligand MC_2H_4 π-type complexes are observed only with copper and gold but not with silver. The IR and UV-visible experiments of McIntosh et al.[17] identified the monoligand complexes MC_2H_4 for all the three metals, but the bi- and triligands were identified only with copper.[8] The more recent IR and Raman study of Merle-Mejean et al.[4] is not in complete agreement with the previous analysis: In contrast with McIntosh et al.,[17] these authors did not find any evidence for the monoligand complexes CuC_2H_4 and AgC_2H_4 in pure ethylene.

Up to now, only few theoretical investigations are available on some of these complexes. Xα calculations performed by McIntosh et al.[17] on the MC_2H_4 (M = Cu, Ag, Au) series failed in describing the observed optical spectrum. RHF calculations performed by Cohen and Basch[18] on the $Ag(C_2H_4)_{1,2}$ complexes did not give any evidence for bound states correlated to $Ag(d^{10}s^1)$. The CuC_2H_4 complex has been investigated through RHF calculations[19,20] and CI calculations that were discussed in detail in an earlier paper.[21]

The latter work was performed with canonical delocalized SCF MO's and concluded that the ground state was a π complex (C_{2v}) while the σ complex (C_s) was found to be higher in energy. Moreover, while the excited states of CuC_2H_4 were found to be chemically bound, the ground state was to be regarded as weakly bound (not bound at the RHF level) due to van der Waals interactions only.

It is well-known that the calculation of intermolecular forces within the supersystem approach with delocalized MO's is very tedious. Indeed, the configurations in the CI cannot be assigned a local character, and dispersion contributions cannot be separated from other physical effects (such as the variation of intrasystem correlation, polarization, charge-transfer contributions) or basis set superposition error. Dispersion contributions are generally much smaller than the other terms (particularly the intrasystem correlation), and any error on the extra terms may turn into unreliable results concerning the van der Waals bonding. It should be stressed that the position of the van der Waals minimum is

(1) See, for example: Parker, S. F.; Peden, C. H. F.; Barrett, P. H.; Pearson, R. G. *Inorg. Chem.* **1983**, *22*, 2813.
(2) For a review see: Zoellner, R. W.; Klabunde, K. J. *Chem. Rev.* **1984**, *84*, 545.
(3) Manceron, L.; Andrews, L. *J. Am. Chem. Soc.* **1985**, *107*, 563.
(4) Merle-MeJean, Th.; Bouchareb, S.; Tranquille, M. *J. Phys. Chem.* **1989**, *93*, 1197.
(5) Huber, H.; Ozin, G. A.; Power, W. J. *Inorg. Chem.* **1977**, *16*, 979.
(6) Hanlan, A. J. L.; Ozin, G. A.; Power, W. J. *Inorg. Chem.* **1978**, *17*, 3648.
(7) Ozin, G. A.; Power, W. J. *Inorg. Chem.* **1978**, *17*, 2836.
(8) Ozin, G. A.; Huber, H.; McIntosh, D. *Inorg. Chem.* **1977**, *16*, 3070.
(9) Grinter, R.; Slotesbury, S. J. *J. Mol. Struct.* **1982**, *80*, 125.
(10) Kasai, P. H. *J. Am. Chem. Soc.* **1982**, *104*, 1165.
(11) Kasai, P. H. *J. Phys. Chem.* **1982**, *86*, 3684.
(12) Chenier, J. H. B.; Howard, J. A.; Mile, B.; Sutcliffe, R. *J. Am. Chem. Soc.* **1983**, *105*, 788.
(13) Howard, J. A.; Sutcliffe, R.; Tse, J. S.; Mile, B. *Organometallics* **1984**, *3*, 859.
(14) Kasai, P. H. *J. Am. Chem. Soc.* **1984**, *106*, 3069.
(15) Kasai, P. H.; McLeod, D., Jr.; Watanabe, T. *J. Am. Chem. Soc.* **1980**, *102*, 179.
(16) Kasai, P. H. *J. Am. Chem. Soc.* **1983**, *105*, 6704.
(17) McIntosh, D. F.; Ozin, G. A.; Messmer, R. P. *Inorg. Chem.* **1980**, *19*, 3321.
(18) Cohen, D.; Basch, H. *J. Am. Chem. Soc.* **1983**, *105*, 6980.
(19) Iloh, H.; Kunz, A. B. *Chem. Phys. Lett.* **1979**, *66*, 531.
(20) Kelber, J. A.; Harrah, L. A.; Jennison, D. R. *J. Organomet. Chem.* **1980**, *199*, 281.
(21) Nicolas, G.; Barthelat, J. C. *J. Phys. Chem.* **1986**, *90*, 2870.

0002-7863/90/1512-5410$02.50/0